Using design principles to systematically plan the synthesis of hole-conducting transparent oxides: Cu₃VO₄ and Ag₃VO₄ as a case study

Giancarlo Trimarchi, Haowei Peng, Jino Im, and Arthur J. Freeman
Department of Physics, Northwestern University, Evanston, Illinois 60208, USA

Veerle Cloet, Adam Raw, and Kenneth R. Poeppelmeier
Department of Chemistry, Northwestern University, Evanston, Illinois 60208, USA

Koushik Biswas[*] and Stephan Lany
National Renewable Energy Laboratory, Golden, Colorado 80309, USA

Alex Zunger
University of Colorado, Boulder, Colorado 80309, USA

In order to address the growing need for p-type transparent conducting oxides (TCOs), we present a materials design approach that allows to search for materials with desired properties. We put forward a set of design principles (DPs) that a material must meet in order to qualify as a p-type TCO. We then start from two prototype p-type binary oxides, i.e., Cu_2O and Ag_2O, and define a large group of compounds in which to *search* for unique candidate materials. From this set of compounds, we extracted two oxovanadates, Cu_3VO_4 and Ag_3VO_4, which serve as a case study to show the application of the proposed materials selection procedure driven by the DPs. Polycrystalline Ag_3VO_4 was synthesized by a water-based hydrothermal technique, whereas Cu_3VO_4 was prepared by a solid-state reaction. The theoretical study of the thermochemistry, based on first-principles electronic structure methods, demonstrates that Cu_3VO_4 and α-Ag_3VO_4 are p-type materials that show intrinsic hole-producing defects along with a low concentration of "hole-killing" defects. Owing to its near-perfect stoichiometry, Ag_3VO_4 has a rather low hole concentration, which coincides with the experimentally determined conductivity limit of 0.002 S/cm. In contrast, Cu_3VO_4 is highly off stoichiometric, $Cu_{3-x}VO_4$ ($x = 0.15$), which raises the amount of holes, but due to its black color, it does not fulfill the requirements for a p-type TCO. The onset of optical absorption in α-Ag_3VO_4 is calculated to be 2.6 eV, compared to the experimentally determined value of 2.1 eV, which brings it to the verge of transparency.

PACS number(s): 71.20.Ps, 71.55.Ht, 74.62.Dh, 61.66.Fn

I. DESIGN PRINCIPLES OF p-TYPE TRANSPARENT CONDUCTING OXIDES

p-type transparent conducting oxides (TCOs) show the attributes of transparency and hole conductivity and are extremely rare yet needed for a variety of technological applications.[1] These attributes seem mutually exclusive but can appear in a material that has a band gap large enough for transparency to the visible light along with an electron chemical potential (Fermi level) E_F near the valence-band maximum (VBM). For a material to be a p-type TCO it must satisfy subtle *design principles* (DPs)[2] which establish precise target values for its optical and transport properties:

(i) *Hole-producing defects* (i.e., electron acceptors) should have shallow levels and low formation energies, making them easy to form either as *intrinsic acceptors* (usually metal vacancies or metal anti-site defects) or as *extrinsic acceptor impurities* soluble in the host compound.

(ii) *"Hole-killing" defects* (i.e., electron donors), usually anion vacancies, should be difficult to form when E_F lies low in the band gap. This condition is more easily met[3] by host materials with a VBM which is sufficiently high in energy, i.e., materials that have low intrinsic work functions, such as tellurides and antimonides.

(iii) The compound should be *thermodynamically stable*, even under conditions that are conducive to high hole concentrations (conditions that create hole-producing defects but avoid hole-killing ones).

(iv) In order to have high *hole mobility* to sustain large p-type conductivity, one needs light hole effective masses (m_h^*).

(v) The *optical band gap* must be equal to, or larger than, 3.1 eV to guarantee transparency to the visible light. Note also that the intraband absorption from deeper valence-band states to the E_F should be weak so as not to curtail transparency.

Finding solids that meet these DPs amounts to performing a multi-objective[4] optimization of the properties associated with the DPs as functions of chemical composition and crystal structure of the material. So far, though, it has been mostly the DP on the optical band gap that has guided the selection of candidate TCO materials (both p- and n-type) with the remaining DPs receiving less attention during materials screening.

Figure 1 illustrates the application of the above DPs to generic binary AO and BO host materials. In the upper panel the binaries are compared in terms of the ranges of oxygen chemical potentials in which they are thermodynamically stable. The lower panel shows the oxygen-vacancy formation energy as a function of electron chemical potential, and the position of the charge transition level of the hole-killing defects relative to the band gap. These graphs illustrate how difficult it could be to attain *all* the DPs in one binary oxide. In practice,
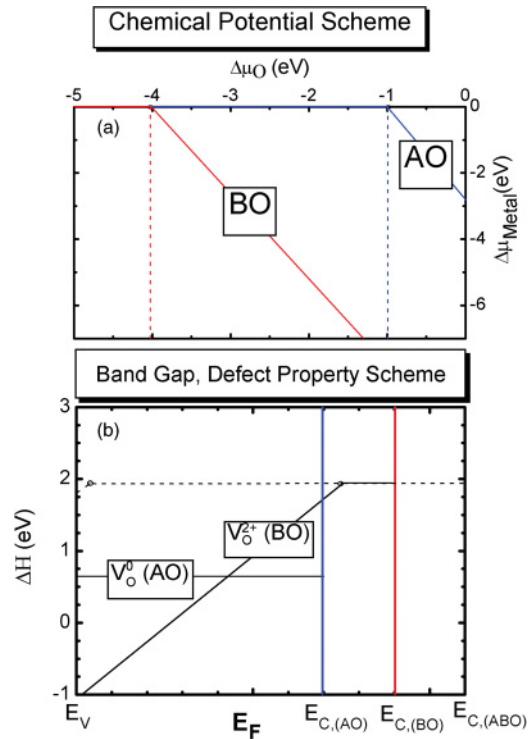
FIG. 1. (Color online) Schematic view of the design principles of thermodynamic stability, formation energy of hole-producing and hole-killing defects, and band gap in the binary *A*-O and *B*-O oxides that are consider for mixing to form a ternary *A*-*B*-O compound.

one observes the existence of two classes of binary compounds that are qualitatively distinct with respect to their ability of complying with the DPs. On the one hand, binary systems such as Ag_2O and Cu_2O, referred to here as "*A*-O oxides," are stable within a range of oxygen chemical potential ($\Delta\mu_O$) corresponding to very oxygen-rich conditions (i.e., very high oxygen partial pressures and exceedingly low temperatures). In these systems the cation vacancy, a hole-producing defect, has a small formation energy and is negatively charged for a Fermi level that lies low in the gap. Furthermore, these systems tend to have the (+2/0) transition level of the oxygen vacancy, a hole-killing defect, close to the VBM. Therefore, this defect does not release electrons that compensate the hole-producing defects. Yet these *A*-O oxides tend to have relatively small band gaps and low formation energies of the hole-killing anion vacancy, both properties that counteract TCO-ness.

On the other hand, there are oxides such as TiO_2, Sc_2O_3, and V_2O_5, referred to here as "*B*-O oxides," which are stable in a larger range of $\Delta\mu_O$, corresponding to oxygen partial pressures and temperatures easily achievable in synthesis, and which have larger band gaps than the *A*-O oxides. These *B*-O oxides usually show relatively large formation energies of the hole-killing defect, a feature that favors high hole conductivity. However, in such materials the transition energy level of the electron-donor defect tends to be well inside the gap, which entails that this defect will release electrons (and compensate

holes) when the Fermi level is near the VBM. Moreover, these *B*-O oxides might have hole-producing defects with an undesired large formation energy.

Since no single binary compound appears to meet all the DPs, the search for optimal *p*-type TCOs has moved into surveying groups of ternary materials. The first *p*-type TCO to be identified was the $CuAlO_2$ delafossite.[5] Starting from $CuAlO_2$, other Cu-based delafossites have been obtained by substituting Al with several trivalent cations.[6–9]

A few other Cu-based compounds outside the structural family of the delafossites have been considered as candidate hole-conducting TCOs. The investigated systems include[10] $SrCu_2O_2$ and structurally related compounds derived by substitution of the divalent cation with other second-column elements. The oxo-chalcogenide[11] LaCuOS represents the prototype of a group of layered materials in which La is substituted by other rare-earth elements or selected trivalent atoms such as Bi,[12] and other chalcogen atoms might be used in place of S. More recently, there has been some attention directed to layered systems[13,14] as $(Cu_2S_2)(Sr_3Sc_2O_5)$, formed by stacking layers of copper sulfide and strontium scandate. Several of these candidate *p*-type TCOs have been selected by inspecting databases of known inorganic compounds, such as the Inorganic Chemistry Structure Database (ICSD),[15,16] and, following chemical intuition, toward target properties. These efforts to find unique *p*-type TCOs follow the general idea to modify simpler (e.g., binary) *p*-type compounds by mixing these with other compounds in order to increase the band gap (reach transparency) in the resulting phase.

Here, we formulate a systematic strategy to search for unique candidate materials which meet the design requirements of *p*-type TCOs. We proceed from the hypothesis that combining an *A*-O with a *B*-O oxide might produce ternary "*A*-O/*B*-O" materials with enhanced TCO properties relative to the parent binary oxides. We articulate our strategy to search this space of *A*-*B*-O oxides in three steps: (1) Select *A*-O compounds that show good hole conductivity. Only few such materials exist; we choose here Cu_2O and Ag_2O, which are the prototype *p*-type oxides. (2) Select *B*-O systems that have larger band gaps and are stable in a broader range of oxygen chemical potentials than the *A*-O compounds. (3) Define a space of candidate ternary *A*-O/*B*-O materials and search it in order to find the optimal ones. This space of *A*-O/*B*-O compounds includes both known systems, which are reported in libraries of inorganic compounds such as the ICSD, so far not considered as *p*-type TCOs, and compounds for which synthesis has not yet been proposed and/or attempted. The ternary oxides identified by the scan of a nontrivially large materials space are then assessed *vis à vis* the DPs by detailed theoretical characterization, synthesis, and property measurements.

The search process of step (2) applied to large spaces of materials, such as the one defined in step (1), will provide a rational basis for planning the synthesis of alternate compounds, not only with TCO functionality. In the following three sections, we describe this three-step process of materials design by taking as a case study the identification and assessment of ternary $(A_2O)_n(B_2O_v)_m$ oxides with $A = Cu$ and Ag, and $B = V$, i.e., Cu_3VO_4 and Ag_3VO_4.

II. ASSESSMENT OF THE BASELINE *p*-TYPE BINARY OXIDES Cu₂O AND Ag₂O AGAINST THE DPs

A. Thermodynamic stability of the host binaries

For a binary oxide A_nO_m to be thermodynamically stable the chemical potentials ($\Delta\mu_\alpha$) of the elemental constituents must satisfy the following relations:

$$n\Delta\mu_A + m\Delta\mu_O = \Delta H_f(A_nO_m), \quad (1a)$$

$$\Delta\mu_A \leqslant 0, \quad \Delta\mu_O \leqslant 0, \quad (1b)$$

$$n'\Delta\mu_A + m'\Delta\mu_O \leqslant \Delta H_f(A_{n'}O_{m'}). \quad (1c)$$

The chemical potential μ_α of a species α is specified by the difference $\Delta\mu_\alpha$ between μ_α and the chemical potential μ_α° of the reference phase of the species α at standard conditions. Equation (1a) expresses the condition of thermodynamic equilibrium of the target A_nO_m compound with its constituents; here, $\Delta H_f(A_nO_m)$ is the heat of formation of A_nO_m with respect to the reference phases of the elemental constituents. Inequalities (1b) express the fact that the chemical potentials $\Delta\mu_\alpha$ must be negative in order to avoid precipitation of the stable phases of the elemental constituents. Inequality (1c), which originates from the condition that *all* possible competing phases $A_{n'}O_{m'}$ with different stoichiometries must be unstable with respect to phase decomposition, further restricts the ranges of chemical potentials at which A_nO_m can form without simultaneous formation of secondary phases. Clearly, Eq. (1a) leaves only one chemical potential as a free parameter. Here, we consider the oxygen chemical potential $\Delta\mu_O$ as the independent variable, as it can be directly controlled by the temperature and the oxygen partial pressure pO_2 during synthesis. Once the interval of chemical potentials of the elements allowed for the formation of a desired compound are determined, one can readily obtain the range of optimal oxygen partial pressures pO_2, as a function of temperature, at which to run reactions of synthesis of that compound. The heats of formation of all the binary and ternary compounds considered in this paper have been calculated by the GGA + U scheme. In the Appendix we provide further details of the GGA + U scheme used and the values of the parameters that were set in these calculations.

Figures 2(a) and 2(b) show the ranges of Ag and Cu chemical potentials ($\Delta\mu_{Ag}$ and $\Delta\mu_{Cu}$) as functions of $\Delta\mu_O$ in which Ag₂O and AgO [Fig. 2(a)], and Cu₂O and CuO [Fig. 2(b)] are thermodynamically favorable. These ranges of chemical potentials for each phase are calculated via expressions (1). In each graph, we also plot the thermodynamically allowed chemical potentials for the binary vanadium oxides V₂O₅ and V₂O₃ as functions of $\Delta\mu_O$. Here, the chemical potentials μ_α° of all elements and the heat of formation (ΔH_f) of the compounds are calculated via GGA + U total-energy calculations. Ag₂O and Cu₂O crystallize in the cuprite structure-type (the crystal structures of AgO, CuO, V₂O₅, and V₂O₃ are given in the Appendix.)

In the plots of Fig. 2, according to the dependence[17] of $\Delta\mu_O$ on T and pO_2 (see the Appendix), moving from higher to lower $\Delta\mu_O$ corresponds to going from oxygen-richer to oxygen-poorer conditions, i.e., from higher to lower pO_2. Also, going from oxygen-richer conditions to oxygen-poorer ones corresponds to moving toward reducing conditions. One
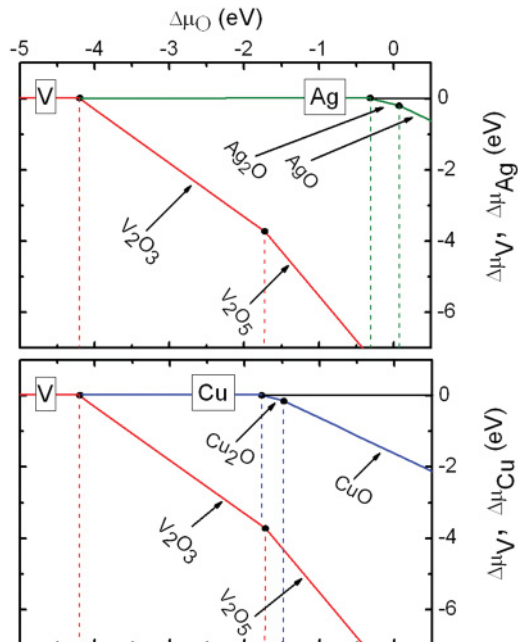

FIG. 2. (Color online) Calculated thermodynamic stability plot of the binary phases of Ag-O (i.e., Ag₂O and AgO), Cu-O (i.e., Cu₂O and CuO), and V-O (i.e., V₂O₅ and V₂O₃). Moving from $\Delta\mu_O = 0$ to more and more negative values, $\Delta\mu_O$ is equivalent when going from O-rich to O-poor synthesis conditions.

observes that at highly oxidizing conditions (large $\Delta\mu_O$), the stable forms of Cu and V oxides are those with the metal in the highest oxidation state. In the Ag-oxide case, only Ag₂O, with the Ag(I) oxidation state, is predicted to be stable. The ranges of chemical potentials in which Ag₂O and Cu₂O are stable are comparable in extension yet they correspond to rather different conditions of pO_2 and T. Indeed, the narrow interval of $\Delta\mu_O$, with the upper bound at $\Delta\mu_O = 0$, in which Ag₂O is stable (see Fig. 2) corresponds to high pO_2 and low temperatures, which are difficult conditions to attain in standard synthesis processes. The range of stability of Cu₂O (see Fig. 2) is limited by the formation of CuO but corresponds to oxygen partial pressures and temperatures easily reached in standard solid-state synthesis. The $\Delta\mu_O$ ranges of Ag₂O and Cu₂O both fall entirely within the much larger interval in which V₂O₅ is stable, so we can expect the formation of stable ternary compounds such as Cu₃VO₄ and Ag₃VO₄.

B. Intrinsic defects, hole generation, and hole densities in Cu₂O and Ag₂O

The formation energy $\Delta H_{D,q}$ of a point defect D in the charge q state is given by the expression[3,18,19]

$$\Delta H_{D,q}(E_F,\mu) = [E_{D,q} - E_H] + q(E_V + \Delta E_F) + n_\alpha(\mu_\alpha^\circ + \Delta\mu_\alpha). \quad (2)$$

The first term on the right-hand side in Eq. (2) is the excess energy of the defect D chemically bound to the host material; the second is the energy of the charge q added to (or removed from) an electron reservoir with chemical potential $E_F = E_V + \Delta E_F$, where E_V is the energy of the VBM of the host; the last term represents the energy of the atom of species

α added to or removed from a reservoir of that species with chemical potential $\mu_\alpha = \mu_\alpha^\circ + \Delta\mu_\alpha$. The charge transition level $\varepsilon(q/q')$ between two charge states q and q' of a defect D is defined by the electron chemical potential E_F for which the formation energies $\Delta H_{D,q}$ and $\Delta H_{D,q'}$ of D, respectively for the q and q' charge states, are equal. According to this definition one obtains the following expression:

$$\varepsilon(q/q') - E_V = [\Delta H_D(E_V; q') - \Delta H_D(E_V; q)]/(q - q'), \quad (3)$$

where the energy level $\varepsilon(q/q')$ is referred to the energy E_V of the VBM. The chemical potentials $\Delta\mu_\alpha$ of oxygen and of the metal species in Eq. (2) are set by the conditions, given by relations (1), for the thermodynamic stability of the A_2O compound in equilibrium with reservoirs of the elements. In the Appendix we give a short description of the technical details of the procedure to calculate by the supercell approach the formation energies and the equilibrium concentrations of the defects, and the equilibrium concentrations of the electron and hole carriers that result from the formation of defects in the host material.

Figure 3 shows the calculated formation energies of the oxygen vacancy, V_O, and the metal vacancies in Ag_2O and Cu_2O as functions of E_F. These defects are, respectively, the main intrinsic hole-killing and hole-producing defects in Ag_2O and Cu_2O. In these figures we also show the formation energy of the oxygen and vanadium vacancies in V_2O_5. These formation energies are calculated at oxygen-rich and at oxygen-poor conditions. These conditions represent, respectively, the most oxidizing ($\Delta\mu_O = 0$) and the most reducing (lowest $\Delta\mu_O$) conditions at which each binary is stable according to the stability plot of Fig. 2. The defect formation energies for the Cu_2O in Fig. 3 are taken from Ref. 20. One notes that the neutral cation vacancies V_{Ag}^0 and V_{Cu}^0 have the $\varepsilon(0/-)$ transition level ~ 0.2 and 0.4 eV above the VBM, respectively. So these defects will be electrically active for a E_F in the band gap.

Both in Ag_2O and Cu_2O the V_O oxygen vacancy has a formation energy comparable to that of the neutral vacancy of the noble metal (in fact, below that of V_{Ag} in Ag_2O) under oxygen-rich conditions. At the same time, though, the V_O vacancy is electrically neutral for any value of the Fermi level in the gap, since the $\varepsilon(+/0)$ charge transition level is located just below the VBM. Thus, the V_O does not act as a hole-killing defect which removes from the valence band the holes originating from the noble-metal vacancy. In V_2O_5, instead, the formation energy of the neutral V_O^0 at O-rich conditions is more than 1.0 eV higher than in Ag_2O and Cu_2O. But when E_F lies low in the gap, V_O^{2+} has low ΔH, causing the production of electrons and, thereby, hole compensation. The formation energy of the vanadium vacancy in V_2O_5 is instead exceedingly high and these defects can be neglected.

From the calculated formation energies of the native defects of Ag_2O and Cu_2O one finds that these oxides are intrinsic p-type conductors. Raebiger *et al.* in Ref. 20 showed that the V_{Cu} defect is the dominant one in Cu_2O, with a concentration at O-rich conditions of $\sim 10^{20}$ at 1000 K. The concentration of V_O defects is found at O-rich conditions up to three orders of magnitude lower than that of V_{Cu} defects. These authors observe that the V_{Cu} defects are responsible for the
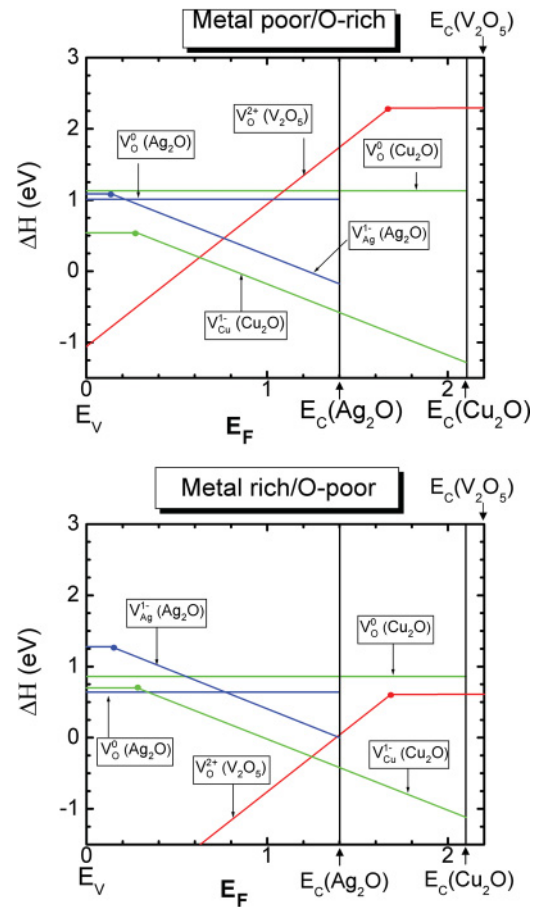

FIG. 3. (Color online) Calculated formation energy and charge transition levels of the main donor and acceptor defects in Cu_2O, Ag_2O, and V_2O_5, i.e., respectively, V_O and the cation vacancy. The defect energies for Cu_2O are taken from Raebiger *et al.* (Ref. 20). The zero of the energy is set at the VBM while $E_c(Ag_2O)$, $E_c(Cu_2O)$, and $E_c(V_2O_5)$ (and the corresponding vertical lines) indicate the position of the CBM. The O-rich/metal-poor and O-poor/metal-rich conditions are defined respectively by the highest and lowest values of the interval of oxygen-chemical potentials shown in Fig. 2 in which Cu_2O, Ag_2O, and V_2O_5 are thermodynamically stable.

Cu off-stoichiometry of Cu_2O and that the hole concentration as a function of the growth temperature follows closely the concentration of the V_{Cu} hole producers. Here, we find that also Ag_2O is a p-type material, but even at O-rich conditions the V_{Ag} and hole content in Ag_2O is predicted to be negligible. Indeed, one has to reach pO_2 many thousands of times higher than that at room condition in order to get to hole concentrations of the order of 10^{12}, a fact that confirms the stoichiometric nature of Ag_2O.

When we mix a "B-O" oxide with Ag_2O or Cu_2O we want to transfer from Ag_2O or Cu_2O to the resulting compound the feature of showing an equilibrium concentration of hole-producing defects without introducing possible hole-killing defects that might originate from the "B-O" oxide. Mixing Ag_2O and Cu_2O with V_2O_5 might result in materials which inherit from Ag_2O and Cu_2O electron acceptors with a low formation energy and $\varepsilon(0/-)$ located in the gap near the VBM. In such oxovanadates the V_O vacancy might still be electrically inactive because of the donor level $\varepsilon(+/0)$ located below the
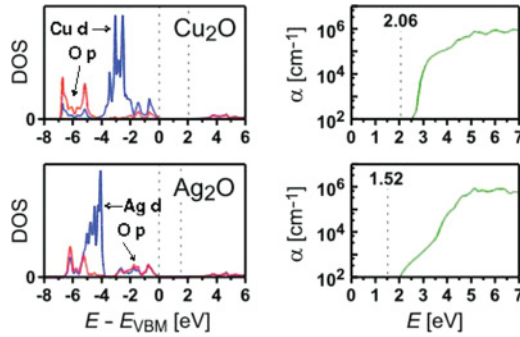
FIG. 4. (Color online) Calculated density of states (left-hand panels) and absorption spectrum (right-hand panels) of the prototypical p-type oxides Cu_2O and Ag_2O obtained by the GW method. Blue (dark gray) and red (gray) lines correspond to the noble-metal d and O p partial DOS, respectively. The zero of the energy is set at the VBM, which is indicated together with the CBM by a dashed vertical line. Owing to its indirect character, the onset of optical absorption is at higher energy than the electronic band gap (shown by dashed lines).

VBM. At the same time, these oxovanadates might inherit from V_2O_5 a high formation energy for V_O that makes this defect more difficult to form than in the Ag_2O and Cu_2O.

C. Band-structure properties of Cu_2O and Ag_2O: Optical properties of the binaries

Figure 4 shows the calculated density of states and the absorption spectrum obtained within the framework of the GW (Ref. 21) method (see the Appendix for the technical details of the calculations of the excited states properties). Both in Cu_2O and Ag_2O the p and d orbitals fall into a similar energy range and their interaction results into a large hybridization effect. The d states of the noble-metal atoms are at a higher energy than the p states of oxygen, therefore, the p-d hybridization produces dispersed d-like bands at the valence-band maximum. These d-like bands show small hole effective masses, as reported in Table I. It is notable that the band gap of Ag_2O ($E_g = 1.52$ eV) is smaller than that of Cu_2O ($E_g = 2.06$ eV), even though the Ag-d states in the atom lie lower in energy than the Cu-d ones (relative to the O-p band—see Fig. 4), a fact from which one would expect a deeper VBM and hence a larger band gap. However, the extended Ag-5s orbitals overlap strongly due to

TABLE I. Calculated minimum electron band gap E_g, optical gap E_g^{opt} (both obtained with the GW method), and DOS effective mass $\frac{m_{DOS}^*}{m_e}$ (determined from the electronic structure calculated via the GGA + U method) of the binary and ternary Ag and Cu oxides considered in this paper. We also report the calculated values of these quantities for the p-type TCO $CuAlO_2$ (delafossite).

	E_g (eV)	E_g^{opt} (eV)	$\frac{m_{DOS}^*}{m_e}$
Cu_2O	2.06	2.5	3.7
Ag_2O	1.52	2.0	2.4
Cu_3VO_4	0.98	1.2	5.6
α-Ag_3VO_4	2.38	2.6	2.2
β-Ag_3VO_4	2.67	3.3	4.2
$CuAlO_2$	4.45	5.0	10.0

the exceptionally small metal-metal distances in the cuprite lattice,[20] forming a very dispersive Ag-s-like conduction band with a very low-lying conduction-band minimum (CBM), causing the smaller band gap in Ag_2O. Since the optical transition matrix elements between the valence band and the Ag-5s-like conduction band are rather small (the VBM-to-CBM transition is symmetry forbidden at the zone center), strong absorption (i.e., absorption with a coefficient larger than 10^4 cm^{-1}) occurs only at energies higher than 3.5 eV, a fact that leads to the large difference between the fundamental and optical band gaps in Ag_2O (see Fig. 4 and Ref. 22). In Cu_2O, the optical excitation at the fundamental band gap E_g is also forbidden, but strong optical absorption occurs already at energies slightly above E_g, because the s-like conduction band is less dispersive than in Ag_2O (the Cu-4s orbitals in Cu_2O overlap less than the Ag-5s orbitals in Ag_2O).

III. SELECTION OF UNIQUE CANDIDATE TERNARY p-TYPE TCOs

A. Definition of the search space

The design principles for p-type TCOs can be applied to a wide range of materials. For instance, recently there has been an application of these to a spinel oxides (see Perkins et $al.$[23]). One can select several A-O oxides as baseline p-type compounds to define families of materials to explore for identifying unique systems that meet the DPs. A possible baseline p-type oxide is NiO, from which one could derive a rather rich space of compounds as the NiO-CoO one. In the present work we applied the DPs to a selected set of materials; we picked Ag_2O and Cu_2O as baseline A-O p-type oxides from which we defined alternate ternary A-B-O oxides via the equation

$$n A_2O + l B_2O_v \rightarrow A_{2n}B_{2l}O_{n+lv}. \qquad (4)$$
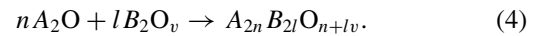
In Eq. (4), the degrees of freedom to specify a compound are represented by the species of the B element, by its valence state v, and by the l/n ratio of A_2O and B_2O_v that yields a thermodynamically stable A-B-O compound. These three parameters define the search space for different phases.

For each B one should determine the full set of stable compounds generated by Eq. (4) and their relative crystal structure. As shown by the over 16 000 ternary mixed metal oxides in the ICSD, the large majority of the elements in the periodic table have been considered for defining A-B-O systems. Yet the limited stability of Ag_2O has made it difficult to fully explore the vast set of Ag-B-O systems. Therefore, a large pool of compounds in this group remains to be explored via planned synthesis driven by DPs. The set of Cu-B-O oxides has been explored in a more complete fashion, owing to the higher stability of the copper oxides compared to the silver ones. Nevertheless, many stable compounds, including some of potential interest as TCOs, to the the best of our knowledge, have received no attention so far.

B. Selection of candidate p-type TCOs driven by the DPs: Ag_3VO_4 and Cu_3VO_4 as a case study

We are interested in illustrating the steps of the materials design process starting from the DPs based on a case study

that includes two compounds: Ag_3VO_4 and Cu_3VO_4. These are generated by Eq. (4) and are selected according to the type of electronic structure that might suit the DPs. We observe that if the B atom in B_2O_v does not contribute electronic states in the same range of energies as the d bands of Ag and Cu (see Fig. 4), then once mixed with the A-O compounds it would not alter the valence band of the A-O materials. The B_2O_v compounds where B is an early transition metal, such as V, Nb, and Ta, are characterized by a d^0 electronic configuration and meet such a requirement. In the A-B-O systems the d levels originating from the B metal will lie at the bottom of the conduction band, as it happens in the B_2O_v binaries because of the d^0 configuration. Therefore, the electronic states originating from the B species in a A-B-O compound might have little influence on the ability of the d-like bands originating from Ag or Cu to sustain good hole mobility. Moreover, an early transition metal B has the ability of forming stronger B-O bonds than Ag and Cu, thus making it energetically less favorable to form the O vacancy, which, being an electron donor, is undesired in a p-type material. In the case of $B = $ V, this fact is reflected by the large stability range of the vanadium binary oxides as a function of $\Delta\mu_O$, a range much larger than that of Cu_2O and Ag_2O. The oxovanadates that would result from the reaction of Cu_2O with V_2O_5 and of Ag_2O with V_2O_5 represent good examples of A-O/B-O systems selected via the previous rules. Among the Cu and the Ag oxovanadates, Ag_3VO_4 and Cu_3VO_4 are stable compounds with known crystal structures, thus they represent a good case study of the application of Eq. (4) to generate materials which might meet the DPs of p-type TCOs.

C. Crystal structures of Ag_3VO_4 and Cu_3VO_4

To date, three crystalline polymorphs of Ag_3VO_4 have been reported: α-Ag_3VO_4, depicted in Fig. 5(c), whose synthesis and refinement have been reported in Refs. 24 and 25, β-

FIG. 5. (Color online) (a) Cuprite structure type (Cu_2O and Ag_2O), (b) shcherbinaite structure type (V_2O_5), (c) α-Ag_3VO_4 structure type, and (d) famatinite structure type (β-Ag_3VO_4 and Cu_3VO_4). The gray spheres correspond to the Ag or Cu atoms, the green (dark gray) spheres correspond to the V atoms, and the red (light gray) spheres correspond to the O atoms.

Ag_3VO_4, which has the famatinite[26,27] structure-type depicted in Fig. 5(d), and γ-Ag_3VO_4 (not shown in Fig. 5) in which the O atoms randomly occupy the tetrahedral interstitials sites of the fcc sublattice that Ag and V form in the α-Ag_3VO_4 and β-Ag_3VO_4 phases. Based on an exhaustive scan of the ICSD, we observed that the crystal structure of α-Ag_3VO_4 represents a unique structure type among ternary A_3BX_4 compounds. Both the α-Ag_3VO_4 and famatinite crystal structures can be derived from the fcc lattice. In both structures, the A and B cations order along the [201] direction of the fcc lattice with the A_3B_1 stacking sequence; the O atoms, instead, occupy tetrahedral interstitial sites of the fcc cation lattice, forming distinct patterns in α-Ag_3VO_4 and famatinite. While in famatinite all cation sites are tetrahedrally coordinated, in α-Ag_3VO_4 the Ag sites retain fourfold, but not tetrahedral, coordination geometries, characterized by linear O-Ag-O bonding units.

α-Ag_3VO_4 was found[24] to be stable up to 365 K; the famatinite-phase β-Ag_3VO_4 (Ref. 24) is stable between 365 and 687 K. Thin films of β-Ag_3VO_4 have been reported by Hirono *et al.*[28] to reversibly transform to α-Ag_3VO_4 under the influence of 330-nm light at 25 °C. In contrast to Ag_3VO_4, Cu_3VO_4 has been synthesized only in the famatinite structure by Bernard *et al.* (see Ref. 29). We have also made several attempts to synthesize Cu_3VO_4 at low temperatures in the α-Ag_3VO_4 structure type, but this phase was never observed, which is strong indication that the famatinite structure type is the only stable one for this system.

IV. ASSESSMENT OF Cu_3VO_4 AND Ag_3VO_4

A. Thermodynamic stability of the Cu_3VO_4 and Ag_3VO_4 ternaries

1. First-principles predictions

The conditions of thermodynamic stability of binary compounds given by expressions (1) are extended to ternary A_3BO_4 oxides by including the conditions of stability with respect to phase separation into ternary compounds at other stoichiometries:

$$3\Delta\mu_A + \Delta\mu_B + 4\Delta\mu_O = \Delta H_f(A_3BO_4), \quad (5a)$$

$$\Delta\mu_A \leqslant 0, \quad \Delta\mu_B \leqslant 0, \quad \Delta\mu_O \leqslant 0, \quad (5b)$$

$$n'\Delta\mu_A + m'\Delta\mu_O \leqslant \Delta H_f(A_{n'}O_{m'}), \quad (5c)$$

$$l'\Delta\mu_B + m'\Delta\mu_O \leqslant \Delta H_f(B_{l'}O_{m'}), \quad (5d)$$

$$n'\Delta\mu_A + l'\Delta\mu_B + m'\Delta\mu_O \leqslant \Delta H_f(A_{n'}B_{l'}O_{m'}). \quad (5e)$$

Equation (5a) represents a plane in the three-dimensional space whose Cartesian axes correspond to the chemical potentials of the elements and, therefore, leaves the chemical potentials of two of the three species as independent variables. Conditions (5b) define on this three-dimensional plane a triangle corresponding to the negative chemical potentials of the elements. Such a region on the Eq. (5a) plans is represented in Figs. 6(a) and 6(b) via its two-dimensional projection onto the plane of the $\Delta\mu_{Ag}$ ($\Delta\mu_{Cu}$) and $\Delta\mu_V$ chemical potentials at $\Delta\mu_O = 0$ (oxygen-rich conditions). Moving along the $\Delta\mu_O$ axis to more negative values (i.e., toward increasingly oxygen-poorer conditions) the area of this triangular two-dimensional projection decreases. The conditions (5c)–(5e) express the requirement of stability of the target compound
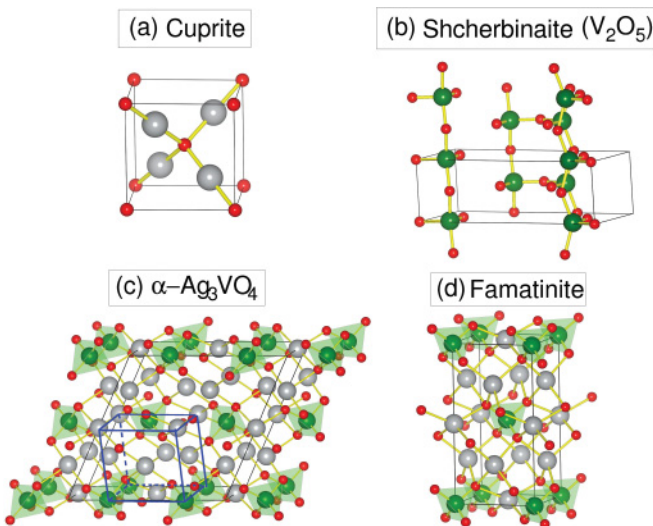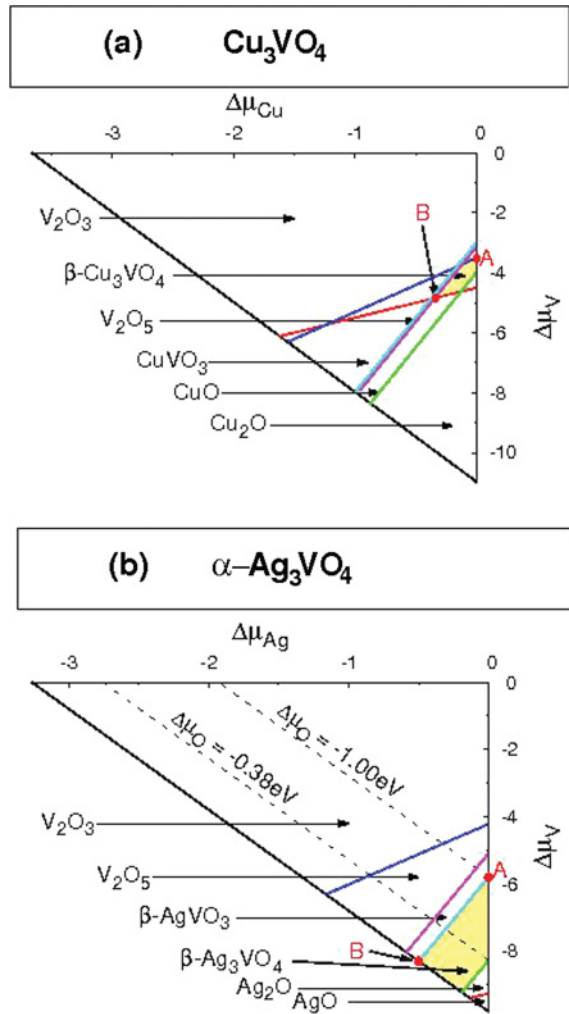
FIG. 6. (Color online) Calculated ranges of chemical potentials of the elements in which Ag_3VO_4 and Cu_3VO_4 are thermodynamically stable. This range of stability is identified excluding the regions of chemical potentials in which competing phases are stable. The arrows associate one of the competing phases (i.e., the constituent binaries and ternary compounds at other compositions) to the region of the chemical potential space in which that phase is stable. The chemical potentials at the points A and B correspond to the oxygen-poor/silver-rich conditions and to the oxygen-rich/silver-poor conditions, respectively.

with respect to phase decomposition into competing binary and ternary phases. Each of the inequalities (5c)–(5e) introduces boundaries for the region of allowed chemical potentials, excluding a section of the stability triangle defined by Eq. (1a) and conditions (1b). To draw these ranges, we considered as phases competing in stability with Ag_3VO_4 the noble-metal binaries Ag_2O and AgO, the vanadium oxides V_2O_3 and V_2O_5, and the $AgVO_3$ ternary vanadate. The analogous set of competing Cu binary oxides and oxovanadates was considered to determine the range of stability of Cu_3VO_4.

The stability plot of Cu_3VO_4 in Fig. 6(a) indicates that this compound forms within a narrow range of chemical potentials. Therefore, no significant extension of the range of $\Delta\mu_O$ available to the binary Cu_2O (see Fig. 2) is achieved in this ternary material. The oxygen partial pressures and

temperatures that correspond to the allowed chemical potentials can be easily reached with standard synthesis methods. From Fig. 6(b) we see instead that Ag_3VO_4 is stable for $\Delta\mu_O$ between 0 and -1.01 eV. This $\Delta\mu_O$ interval corresponds to ranges of temperatures and pressures that encompass much higher temperatures and much lower oxygen pressures than those needed to make Ag_2O. Indeed, Ag_3VO_4 is predicted to be thermodynamically stable at room conditions as well as at pressures and temperatures typical of solid-state and hydrothermal synthesis.

2. Synthesis

Single crystals of Ag_3VO_4 have been prepared by hydrothermal synthesis using hydrofluoric acid (HF) as a mineralizer (see Ref. 25). In contrast, polycrystalline α-Ag_3VO_4 has been made by Dinnebier *et al.* (see Ref. 24) by using a solid-state synthesis at high temperature and high pressure.

In this research, an alternate hydrothermal route using KOH as a mineralizer was developed, which resulted in polycrystalline α-Ag_3VO_4. The advantage of this route is the use of mild temperatures (below 473 K) and low pressures. For successful hydrothermal synthesis, a minimum solubility of 2%–5% of the least soluble compound is necessary.[30] In the case of α-Ag_3VO_4 synthesis, the least soluble compound is Ag_2O (16.2 mg/L for Ag_2O and 640 mg/L for V_2O_5, both in water at 25 °C). Both oxides are amphoteric and dissolve in acidic and basic media. However, in an acidic medium, V^{5+} will be reduced to V^{3+}, so working in the high pH region, where V_2O_5 is present as a VO_4^{3-} anion, is preferable. The use of KOH, a basic mineralizer, enhances the solubility of Ag_2O, which allows the formation of more soluble complexes than with water alone, and creates the required basic medium. Cu_3VO_4 was prepared by a solid-state reaction by reacting Cu_2O and V_2O_5 in a fused-silica tube at 550 °C. To eliminate the Cu_2O excess, a considerable Cu deficiency in the reactant ratio was necessary, which results in $Cu_{3-x}VO_4$ with $x = 0.15$.

3. Phase transition

Dinnebier *et al.* reported in Ref. 24 a phase transition from α-Ag_3VO_4 to β-Ag_3VO_4 at 376 K in vacuum. This phase transition was found at 383 K/358 K by our differential scanning calorimetry (DSC) measurement under a dry nitrogen atmosphere (Fig. 7). A hysteresis (25 K) between heating and cooling in the transition from α to β is observed, owing to the gradual phase change; moreover, the cooling rate is usually
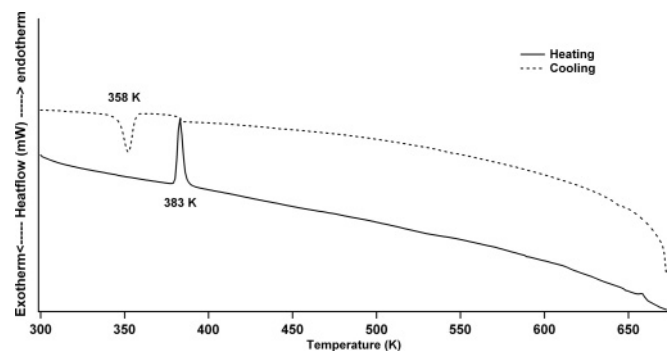

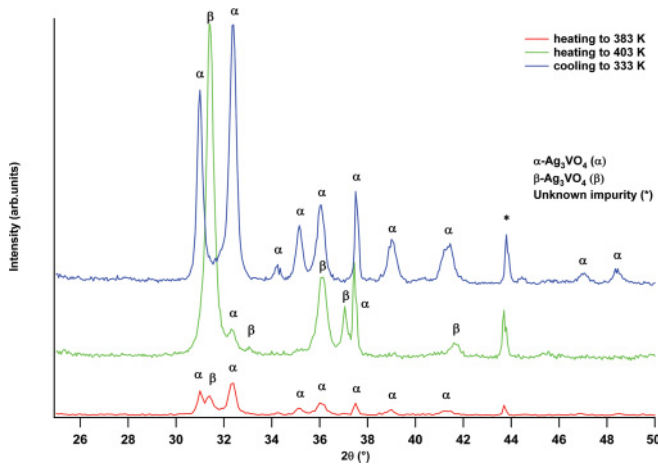FIG. 7. Heating and cooling DSC graphs of α-Ag_3VO_4.

FIG. 8. (Color online) *In situ* high-temperature PXRD analysis of Ag_3VO_4.

slower than the heating rate. Owing to the low transition temperature, the β-Ag_3VO_4 phase can be easily obtained by gently heating the crystals. Upon heating, the color changes from bright red to dark purple for the β-Ag_3VO_4 phase. *In situ* high-temperature powder x-ray diffractometry (PXRD), as displayed in Fig. 8, clearly illustrates the transformation to the β phase. Both phases, α-Ag_3VO_4 and β-Ag_3VO_4, are present at 383 K, which demonstrates the gradual transformation. At 403 K the transformation to β-Ag_3VO_4 is complete, and at 333 K the α phase is present again. In addition, the β-Ag_3VO_4 phase is light sensitive and quickly transforms back to the α-Ag_3VO_4 phase. This phenomenon has been earlier described by Hirono *et al.*[28] These authors stated that irradiation of β-Ag_3VO_4 at 330 nm and 298 K converts the film to α-Ag_3VO_4. The photochromic properties of Ag_3VO_4 and other Ag-containing ternaries have been studied by Hirono *et al.*[31]

B. Intrinsic defects, hole generation, and hole density in Cu_3VO_4 and Ag_3VO_4

Figures 9(a)–9(d) show the formation energies of the cation and oxygen vacancies in Cu_3VO_4 and α-Ag_3VO_4 as functions of E_F calculated by using Eq. (2). The chemical potentials of the elements used in Eq. (2) refer to the most and least oxidizing conditions, respectively, the O-rich condition with $\Delta\mu_O = 0$, and the O-poor condition that corresponds to the minimum $\Delta\mu_O$, and in both cases to the corresponding metal chemical potentials, compatible with the conditions of stability of the target phase imposed by relations (5). The formation energies of the noble-metal vacancies as a function of the electron chemical potential E_F follow in the ternaries a behavior similar to that observed in the Ag_2O and Cu_2O. In both ternaries, the neutral Ag and Cu vacancies have lower formation energies than in the corresponding binaries, with the $\varepsilon(0/-)$ level just above the VBM. The hole-killing defect V_O is, as in the binaries, neutral for any E_F within the band gap, and therefore does not release electrons that would cause hole compensation. Hence, the VO_4 complexes in the ternaries do not induce a shift of the charge transition level of the oxygen vacancies toward the middle of the gap, where it is positioned in V_2O_5. In turn, though, we find a much larger formation
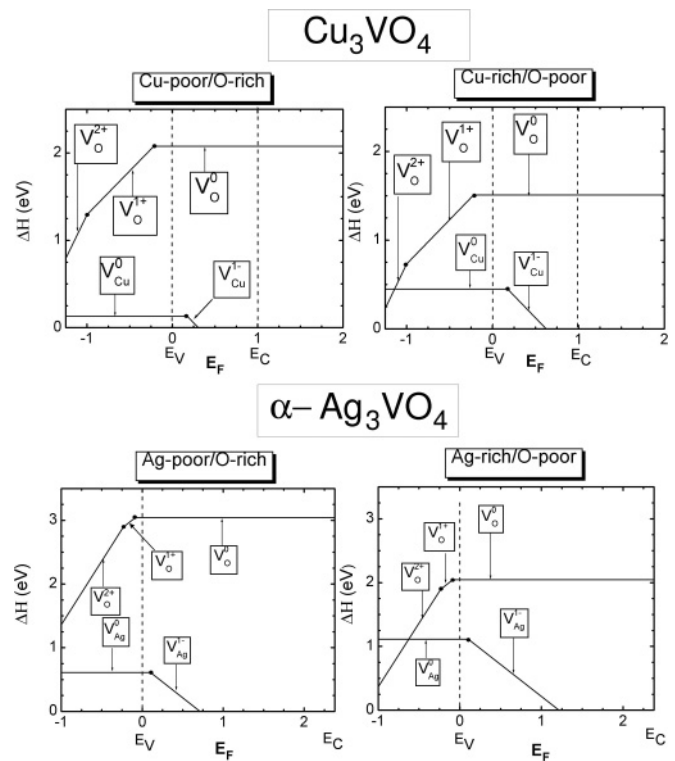

FIG. 9. Calculated defect formation energies of the V_{Ag}, V_{Cu}, and V_O vacancies in Cu_3VO_4 and α-Ag_3VO_4 as functions of the electron chemical potential E_F. The VBM and the CBM are indicated by the E_V and E_C labels, respectively. The metal-rich/oxygen-poor and metal-poor/oxygen-rich conditions are defined by the chemical potentials that correspond to the points indicated by A and B in the thermodynamic stability plots displayed in Figs. 6(a) and 6(b).

energy for the neutral V_O that is related to the increased binding energy of the oxygen to the host due to the strong V-O bonds. The $\Delta H(V_{Cu})$ is rather low in Cu_3VO_4, a fact in accord with the intrinsic copper off-stoichiometry observed in the synthesized material.

As evidenced by the synthesis reaction, Ag_3VO_4 is nearly perfectly stoichiometric. From Fig. 9 we see that the formation energy of the silver vacancy (the main hole-producing defect) is comparable to that in Ag_2O, with the charge transition level close to the VBM. By contrast, the hole-killing V_O has a formation energy larger than in Ag_2O and close to that in V_2O_5. This greatly decreases the equilibrium concentration of hole-killing defects in Ag_3VO_4 with respect to Ag_2O.

Figure 10 shows the equilibrium hole concentration n_h in α-Ag_3VO_4 and β-Ag_3VO_4 as a function of temperature at room pressure (i.e., $pO_2 = 0.2$ atm), obtained according to the procedure outlined in the Appendix. The total concentration of V_{Ag} and the concentration of holes virtually coincide at $pO_2 = 0.2$ atm. This shows that at thermodynamic equilibrium conditions virtually all the acceptor defects are electrically active and not compensated by the O vacancies. The hole concentration n_h (therefore, also the V_{Ag} concentration) reaches 10^{15} cm^{-3} at $T = 383$ K, the temperature of the transition from α- to β-Ag_3VO_4. Such a small amount of holes reflects the negligible off-stoichiometry of α-Ag_3VO_4. We predict that the hole concentration could be significantly
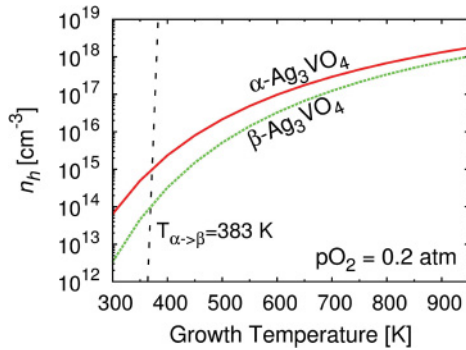
FIG. 10. (Color online) Calculated hole concentration n_h as a function of temperature in α-Ag$_3$VO$_4$(red/solid line) and β-Ag$_3$VO$_4$(green/dashed line). The vertical dashed indicates the transition temperature between the α and β phases of Ag$_3$VO$_4$.

increased increasing the temperature in β-Ag$_3$VO$_4$(e.g., by three orders of magnitude going up to 800 K) if it were possible to stabilize its structure. The hole content and the band gap (described in the next section) in β-Ag$_3$VO$_4$, predicted to be, respectively, larger and wider than in α-Ag$_3$VO$_4$, suggest that β-Ag$_3$VO$_4$ might be transparent to the visible light and have a non-negligible intrinsic content of holes, both desired features in optimal p-type TCOs.

C. Band-structure properties: Optical absorption and hole mobility

1. Optical properties

Figure 11 compares the electronic density of states of α- and β-Ag$_3$VO$_4$ with that of Cu$_3$VO$_4$, all calculated via the *GW* (Ref. 21) method. One immediately notes that the band gap of Ag$_3$VO$_4$ is larger than that of Ag$_2$O. The electronic structure of
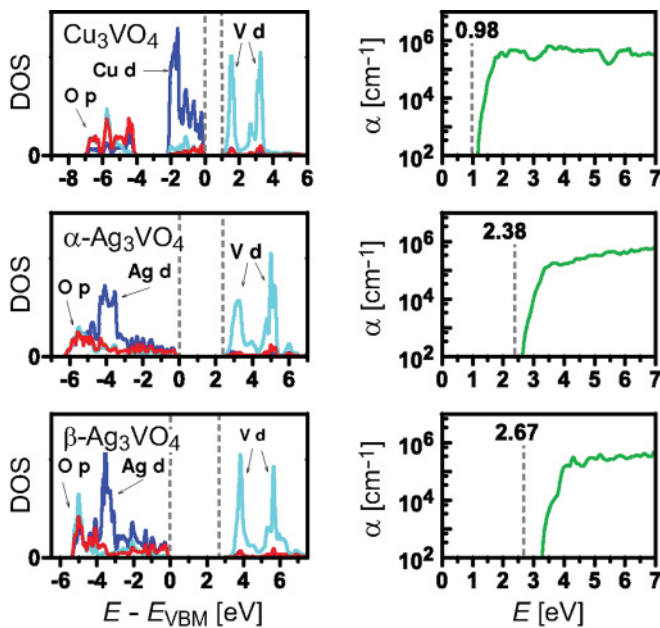

FIG. 11. (Color online) Calculated density of states (left-hand side) and absorption spectrum (right-hand side) of Cu$_3$VO$_4$, α-Ag$_3$VO$_4$, and β-Ag$_3$VO$_4$. The dark blue (dark gray), light blue (light gray), and red (gray) lines show, respectively, the Cu(/Ag)-d, V-d, and oxygen-p partial DOSs.
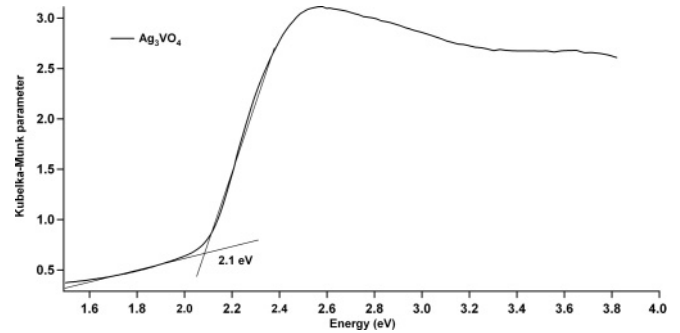

FIG. 12. Measured diffuse reflectance spectrum acquired on a nonsintered Ag$_3$VO$_4$ pellet.

these compounds can be explained in terms of the interaction between the O-p orbitals and the d orbitals of Ag and Cu, respectively, in Ag$_3$VO$_4$ and Cu$_3$VO$_4$. Note that the atomic O p levels are at a much deeper energy in the band gap than the Ag and Cu d levels. In Ag$_3$VO$_4$ the p-d hybridization (and the subsequent splitting of these levels) produces the bands at the VBM, which are dominantly of Ag d type, while the subbands deriving from the O p levels are placed deeper in the valence band, right below the Ag d states. The p-d interaction leads to the reduction of the gap in Ag$_3$VO$_4$ between the Ag d and O p valence subbands near the top of the valence band with respect to that observed in Ag$_2$O.

Cu$_3$VO$_4$ is predicted to be not transparent with a rather small band gap of $\sim$1.0 eV, between the VBM deriving from Cu-d^{10} and the CBM which derives mainly from V-d^0 states. Ag$_3$VO$_4$ has a larger band gap than Cu$_3$VO$_4$ while in the binaries the trend is inverted with Ag$_2$O, which has a smaller gap than Cu$_2$O. The *GW* calculations predict an optical band gap of 2.6 eV for α-Ag$_3$VO$_4$ and of 3.3 eV for β-Ag$_3$VO$_4$. Thus, stabilizing the β structure, e.g., by strain or alloying, could be a design route to achieve full transparency in Ag$_3$VO$_4$ also at higher energies of the visible spectrum.

The acquisition of the diffuse reflectance spectrum has allowed the measurement of the optical band gap of α-Ag$_3$VO$_4$. A pellet was pressed of polycrystalline α-Ag$_3$VO$_4$. The intercept of the two best fitting lines of the two parts of the graph points out the optical band gap. As can be seen in Fig. 12, the band gap of α-Ag$_3$VO$_4$ is 2.1 eV, which is rather small for an oxide semiconductor.

2. Transport properties

In the largest majority of materials, the hole conductivity *cannot* be expressed as $\sigma = \frac{ne^2\tau}{m^*}$, where τ is the relaxation time, n is the carrier concentration, and e is the electron charge. This relation indeed holds only in the case of systems with parabolic and isotropic bands, while in the present materials the bands at the valence band edges are highly nonparabolic. One should then resort to describing the transport properties within the Boltzmann equation scheme, which fully takes into account the non-parabolicity of the bands and the possibility of the presence of several pockets of carriers close to the band extrema. However, this scheme requires to specify the relaxation time τ, which accounts for the dissipation events in the host material and for which a fully *ab initio* calculation is very difficult to perform. Instead, τ is usually treated as

a constant parameter often set to reasonable values inferred from a fit to experimental conductivities of chemically similar materials. A useful effective quantity that captures the features of the full density of states $g(E)$ of a material, but which does not require setting a relaxation time, is the "equivalent" or "density-of-states" effective mass[32,33] m^*_{DOS} defined by the relation

$$\left(\frac{m^*_{DOS}}{m_e}\right)^{3/2} \propto N_v(T) = \int_{-\infty}^{E_{VBM}} g(E) \times \exp\left[-(E_{VBM} - E)/(k_B T)\right] dE.$$

(6)

In this expression, $N_v(T)$ is the so-called effective DOS (Refs. 34 and 35) and is a temperature-dependent quantity through the Boltzmann factor; the quantity m^*_{DOS} is the effective mass which gives within the parabolic band approximation the same $N_v(T)$ which is obtained from the DOS $g(E)$ of the solid that originates from bands with a dispersion that departs from the parabolic one. Clearly, the effective mass m^*_{DOS} does not depend on the relaxation time.

The m^*_{DOS} effective masses at the VBM calculated at $T = 300$ K in Cu_3VO_4 and Ag_3VO_4 are compared in Table I with those in the respective parent binary compounds Cu_2O and Ag_2O. Going from Ag_2O to α-Ag_3VO_4, the VBM m^*_{DOS} decreases slightly from 2.4 m_e to 2.2 m_e but we can expect comparable hole mobilities in the two materials. In β-Ag_3VO_4, instead, the m^*_{DOS} is almost double than that in α-Ag_3VO_4, likely because of a larger O-p character of the energy levels at the VBM. We observe the opposite trend when going from Cu_2O to Cu_3VO_4 with m^*_{DOS} increasing from 3.7 m_e to 5.6 m_e, owing to a sharp increase of the density of Cu-d levels rather localized in energy close to the VBM. In Table I we show the band gap and hole m^*_{DOS} of the prototype p-type TCO, the $CuAlO_2$ delafossite. In this material the band gap is well above the transparency threshold, yet the m^*_{DOS} at the VBM is close to three times larger than it is in Cu_2O.

Standard four-probe measurements on as-prepared pressed pellets of α-Ag_3VO_4 were performed. However, because of the sensitivity limit of the equipment, conductivity values below 0.002 S/cm could not be measured. The upper limit of the conductivity of α-Ag_3VO_4 must therefore be situated in this range.

V. DISCUSSION AND SUMMARY

We addressed the problem of searching for optimal p-type transparent conducting oxides (TCOs) by a materials design approach. We started by laying out the design principles (DPs) that a material must meet in order to qualify as a p-type TCO. In order to define the space of compounds to search, we put forward the hypothesis that the prototype p-type oxides Ag_2O and Cu_2O represent good baseline materials to combine with other binary oxides and derive compounds that might be candidate p-type TCOs. From this set of materials we selected Cu_3VO_4 and Ag_3VO_4 for a case study of the application of the DPs of p-type TCOs. Although these are known materials, they are brought here within the focus of the design of TCOs.

We believe that in order to move from traditional trial-and-error to the rational, deliberate design of unique functional materials, one has to follow a procedure in which (i) DPs are established, (ii) a nontrivial search space is defined, and (iii) the search space is explored in order to find the materials that exhibit optimal properties in accord with the DPs. On the other hand, it is true that an extensive search cannot be tackled when the materials space is too large and the properties that are to be optimized are not easy to calculate due to a numerically cumbersome algorithm. These are potential drawbacks that determine whether a search approach is viable or not, and can be fully assessed only via the survey of a large space of compounds, not in a case study, as in the present one, which is limited only to a few compounds. Yet the DPs that are established at the outset require that the target properties fall within given intervals rather than take global maximum or minimum values, or even fixed target values. There is then a significant probability to retrive optimal compounds even in search space as large as the one defined here. Based on this fact, we strongly believe that the fully *ab initio* search procedure outlined in this work is a viable one and can be implemented by using the new generation of petaflop massively parallel computers that have been coming online in recent years.

Our theoretical and experimental data show that Ag_3VO_4 complies with all of the proposed DPs, except for hole mobility. We predict that Ag_3VO_4 is stable in ranges of oxygen partial pressures and temperatures that are reachable via standard hydrothermal preparation routes. In contrast to Ag_3VO_4, the parent binary Ag_2O oxide is stable only at high oxygen partial pressures and low temperatures which are not routinely achieved in a standard solid-state synthesis. Polycrystalline α-Ag_3VO_4 was prepared by a water-based hydrothermal synthesis in which the use of hydrogen fluoride as a mineralizer is avoided.

The formation energy of the V_O^0 defect in Cu_3VO_4 and α-Ag_3VO_4 is comparable to that in V_2O_5 but higher than in Cu_2O and Ag_2O. The energy of the transition to the V_O^{2+} charge state is below the VBM, similar to what is found in Cu_2O and Ag_2O. Therefore, for any value of the Fermi level in the gap, the V_O defect will be energetically unfavorable and charge neutral, i.e., it does not compensate holes. We found that Ag_3VO_4 is clearly a p-type oxide. However, since Ag_3VO_4 is highly stoichiometric, the intrinsic concentration of cation vacancies is so low that they do not produce the sizable p-type conductivity desired in a p-type TCOs. This result illustrates the need for extrinsic hole dopants to increase the content of holes and the conductivity in α-Ag_3VO_4. Cu_3VO_4 shows a significant equilibrium copper deficiency which results in high hole concentration. However, Cu_3VO_4 is black and therefore not to be considered as a candidate p-type TCO.

Using the *GW* method, we predicted that the optical absorption edges in α-Ag_3VO_4 and β-Ag_3VO_4 are, respectively, at 2.6 and 3.3 eV, therefore at higher energies than in Ag_2O. Diffuse reflectance data show that α-Ag_3VO_4 has an optical band gap of 2.1 eV, in fair agreement with the calculated one, and the red coloration of the samples confirms the incipient transparency. Several factors can contribute to explaining the discrepancy we find between the predicted optical gap and the measured one: (i) the inaccuracy of the *GW* method, which, as discussed in Appendix A 4, might not provide accurate, quantitative predictions of the position of the d orbitals in system such as the ones studied here where the band edges originate from

d orbitals of transition-metal species; the introduction of the on-site nonlocal external potentials, described in Appendix A 4 alleviates this problem; (ii) the experiment is performed at room temperature while the calculation yields a value for the gap at 0 K; (iii) at the actual sample dimensions, the experiment picks up indirect transitions not considered in theory; (iv) excitonic effects (not included in our calculations) increase the intensity of the transition close to the band-gap energy.

β-Ag$_3$VO$_4$ is predicted by the *GW* calculations performed here to be transparent to the visible light, but its absorption spectrum could not be measured because of the crystal structure transition from β-Ag$_3$VO$_4$ to α-Ag$_3$VO$_4$ under cooling. Therefore, it will be interesting to investigate strategies to stabilize β-Ag$_3$VO$_4$ at lower temperatures in order to obtain a transparent oxide that might offer a good baseline to obtain the hole conductivity desired in a *p*-type TCO. However, we should keep in mind that if a discrepancy between the calculated and experimental onset of absorption similar to that observed in the α phase occurs also in β-Ag$_3$VO$_4$, such a phase would still have an optical band gap somewhat smaller than that needed for it to be a TCO, even if this β phase could be stabilized. Moreover, for both phases of Ag$_3$VO$_4$, first-principles calculations and experimental observations indicate a small concentration of holes arising from intrinsic defects in this material, and therefore low conductivities. By contrast, the Cu vanadate Cu$_3$VO$_4$ has too small a band gap to be a TCO, while the rather high density-of-states mass suggests that the mobility in this compound could be rather low, leading to low conductivities.

In sum, although the compounds chosen here for a case study of the validation of the DPs are not TCOs (both are *p*-type conductors while only α-Ag$_3$VO$_4$ is at the verge of transparency), we observe that a search for alternate candidate *p*-type TCOs driven by the application of the DPs proposed in this paper is a promising design route. Furthermore, the proposed DPs represent necessary conditions that a material should satisfy in order to be a *p*-type TCO; therefore, it is mandatory to embed these DPs in any materials design program that aims at identifying unique *p*-type TCOs. This route will therefore be further explored by extending the search to a much larger set of ternary Cu- and Ag-based oxides.

ACKNOWLEDGMENTS

APPENDIX

A. Electronic structure calculation methods

1. Total-energy calculations

We used the GGA + *U* (Ref. 36) method as implemented in the VASP (Refs. 37 and 38) code to calculate the total energy of the bulk phases and the point-defect configurations of the binary and ternary systems considered in this paper.

Standard density functional theory (DFT) often predicts an incorrect phase of transition-metal oxides to be stable, e.g., Ni$_2$O$_3$ is predicted to be more stable[39] instead of NiO. The resulting inaccuracy of the heat of formation calculated by the generalized gradient approximation (GGA) is corrected by employing the GGA + *U* method[36] and by the use of optimized elemental reference energies.[40] The *U* parameters of Ag, Cu, and V used in this work are $U_{Ag} = 6.3$ eV, $U_{Cu} = 5.8$ eV, and $U_V = 2.2$ eV.

Even though V$_2$O$_5$ is a layered structure in which van der Waals interactions are expected to play a significant role, the lattice parameters obtained in the present GGA + *U* description agree with experiments within typical accuracies of GGA (aspherical contributions to the gradient corrections have been taken into account).

2. Dependence of the chemical potential of oxygen on pressure and temperature

The oxygen chemical potential $\Delta\mu_O$ in the gas phase can be controlled by changing the oxygen partial pressure P and temperature T.[17] Employing the tabulated O$_2$ enthalpy $H_0 = 8.7$ kJ mol^{-1} and entropy $S_0 = 205$ J mol^{-1} K^{-1} at standard conditions ($T_0 = 298$ K and $P_0 = 1$ atm), we have

$$\Delta\mu_O(T,P_0) = \tfrac{1}{2}\{[H_0 + \Delta H(T)] - T[S_0 + \Delta S(T)]\}, \quad (A1)$$

where $\Delta H(T) = C_p(T - T_0)$ and $\Delta S(T) = C_p \ln(T/T_0)$. For $T \geqslant 298$ K, we assume the ideal gas law, and use $C_p = 3.5 k_B$ for the constant-pressure heat capacity per diatomic molecule. For P different than P_0, $\Delta\mu_O(T,P) = \Delta\mu_O(T,P_0) + 1/2 k_B T \ln(P/P_0)$.

3. Defect calculations

The total energies of the defect systems were calculated by using finite supercells. It must be questioned whether the DFT calculations have sufficient accuracy to be used in a predictive manner to calculate materials properties related to point defects. In the *n*-type TCOs, for example, DFT band-gap errors and supercell finite-size effects have given huge differences in the predicted formation energies of native defects calculated by different groups and/or different methods, leading to orders of magnitude differences in the equilibrium concentration of native defects expected. Because of this we were careful to apply the following corrections[18,19] to DFT and the supercell calculations. The sizes and shapes of the supercells were set so as to decouple the relaxation of the crystal structure around periodic images of the defect in neighboring cells. Moreover, we applied the techniques explained in detail in Refs. 18 and 19 to correct for the band-filling effect, which originates from the finite size of the supercell, and for the interaction between periodic image charges (in the case of charged defects).

The concentration $c_{D,q}$ of the defect D in the charge state q and with formation energy $\Delta H_{D,q}$ is expressed[18,34,35] by $c_{D,q} = N_{sites} \exp(-\Delta H_{D,q}/k_B T)$. The electron chemical potential E_F is fixed by the charge neutrality condition, which requires that the total charge associated with the free carriers balances the total charge associated with the charged defects. But the concentration $c_{D,q}$ of a charged defect depends on the electron chemical potential E_F via the defect formation energy

$\Delta H_{D,q}$, expressed by Eq. (2). Therefore, at every temperature T, E_F must be determined self-consistently along with $c_{D,q}$, the concentration of electrons $n_e(T)$, and the concentration of holes $n_h(T)$.

4. Excited states and optical properties calculations

We used the *GW* (Ref. [41]) method to calculate the density of states and optical absorption spectra in Figs. [4] and [9], and the band gaps in Table [I]. Nowadays the *GW* method is the state-of-the art approach in calculating the band structure of semiconductors and insulators. Its accuracy has been extensively tested and verified for a large pool of main-group compounds.[42,43] However, larger uncertainties have been observed for the positions of the *d* bands, e.g., in ZnO.[44] In transition-metal compounds, where *d*-like states are close to the band-gap region, the ability of *GW* to provide accurate quantitative predictions for the band structure remains under investigation. In the *GW* calculations performed in this paper[43] we kept fixed the GGA + *U* wave functions and iterated the *GW* energies to self-consistency. We also included local-field effects that go beyond the random-phase approximation.[45] While this procedure predicts quite accurately the band structures of conventional III-V and II-VI semiconductors,[46] we find systematic deviations from experimental data that result from too high *d*-orbital energies in GW for both occupied (e.g. ZnO and Cu_2O) and unoccupied (e.g., TiO_2 and V_2O_5) *d*-shells. Here, we remedied this problem by employing additional nonlocal empirical potentials[47] to lower the *d*-orbital energies. The parameters for the additional potentials (-2.5, -1.5, and -2.8 eV for Cu, Ag, and V) were determined so as to make the calculated band structures consistent with available experimental data on Cu_2O, Ag_2O, and V_2O_5.

B. Crystal structures of the compounds considered in the thermochemistry calculations

To determine the phase stability plots of Ag_3VO_4 and Cu_3VO_4 depicted in Fig. [6], we considered several binary and ternary compounds, each in its low-temperature crystal structure, as possible competing phases formed by the same species as in Ag_3VO_4 and Cu_3VO_4. The total energies of all compounds were calculated for the crystal structure obtained by fully relaxing the lattice vectors and atomic positions starting from their experimental values. We list here the entries in the ICSD that correspond to the experimental crystal structures of the compounds we considered:

V_2O_5: ICSD No. 15798. It crystallizes in the shcherbinaite structure that has orthorhombic *Pmnm* space-group symmetry (No. 59) and two formula units per unit cell.

V_2O_3: It crystallizes in the corundum crystal structure which has the rhombohedral $R\bar{3}c$ space-group symmetry (No. 167).

Ag_2O and Cu_2O: The crystal structure of these compounds is cuprite,[48] which has the cubic $Pn\bar{3}m$ space-group symmetry (No. 224).

AgO: ICSD No. 202055. It has the $I4_1/a$ space-group symmetry and 16 formula units per unit cell. This compound is metastable and can be made in off-equilibrium conditions, e.g., using ozone as a source of oxygen. The polymorph we use

here is the higher-temperature, tetragonal one. In this structure the oxidation number of the Ag ions is Ag^{1+} and Ag^{3+}, a fact that makes Ag_2O_2, rather than AgO, the basic composition unit.

CuO: ICSD No. 16025. It has the monoclinic $C2/c$ space-group symmetry (No. 15), with four formula units per unit cell.

$AgVO_3$: ICSD No. 82079. This compound is also referred to as β-$AgVO_3$; it has the monoclinic *Cm* space-group symmetry (No. 8), and eight formula units per unit cell.

$CuVO_3$: ICSD No. 19046. This compound crystallizes in the ilmenite-type crystal structure with the $R\bar{3}$ space-group symmetry (No. 148).

C. Experimental methods

1. Synthesis

α-Ag_3VO_4 polycrystalline powders were prepared by a water-based low-temperature hydrothermal synthesis. Ag_2O (Fisher Chemical, laboratory grade), V_2O_5 (Alfa Aesar, 99.6% minimum), and KOH (Sigma-Aldrich, >90%, reagent grade) were mixed in a 1 : 0.85 : 2.34 molar ratio and put into a fluoro(ethylene-propylene) (FEP) Teflon pouch. The pouches were heat sealed before loading them into the autoclave. KOH functions as a mineralizer, which will facilitate the dissolution of the metal ions at an increased *p*H. KOH also regulates the amount of water that diffuses into the pouch. Up to seven pouches were placed in a 125-mL autoclave with a Teflon liner, which was backfilled with 50-mL water. The autoclave was closed and heated at 433 K for 50 h and cooled down to room temperature at 0.1 K/min to maximize crystal growth. In order to measure the amount of diffused water, the pouches were weighed before and after hydrothermal synthesis. After the synthesis, the powders were washed three times with distilled water to remove all traces of KOH.

2. Powder x-ray analysis

Powder x-ray diffraction (PXRD) analyses were obtained from a Rigaku XDS 2000 diffractometer with Ni-filtered Cu $K\alpha$ radiation ($\lambda = 1.5418$ Å) at 40 kV and 20 mA. Data were collected between 15° and 65° at a step size of 0.05° and a dwell time of 0.8 s. The experimentally obtained PXD patterns were compared to the JCPDS file of α-Ag_3VO_4 (43-0542) using the Jade9 software suite. The ICSD pattern matched well with the experimentally obtained pattern, except for two small reflections at 27.95° and 29.25°. Powder XRD diffraction data of the bright red crystals of α-Ag_3VO_4 were collected. Figure [13] displays the experimentally obtained XRD pattern compared to the pattern found in the ICSD database (α: 43-0542; β: 43-0543), which are in good agreement. No other phases are observed, from which we can conclude that the powder is pure. The *in situ* high-temperature XRD was performed on a Scintag XDS2000, with a heating stage. The sample was glued to the sample stage with a slow-curing high-temperature-resistant two-component epoxy glue.

3. Optical data

A diffuse reflectance spectrometer was used to obtain data on optical properties such as the band gap. A Perkin-Elmer
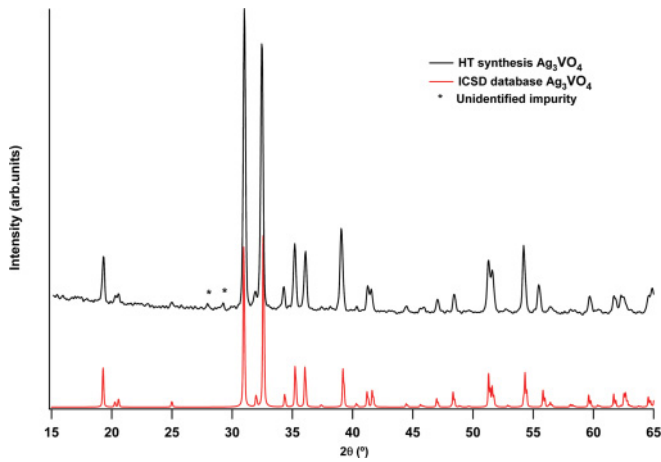
FIG. 13. (Color online) Powder x-ray diffraction pattern of α-Ag_3VO_4 compared to the one reported in the ICSD.

Lambda 1050 instrument with an integrated sphere was used to collect data over the spectral range of 250–800 nm with a data interval of 1 nm. A baseline was collected using a slit width of 2 mm at 650 nm. After the detected light has interacted with the particles of the sample, the absorption spectrum can be extracted from the raw diffuse reflectance data. This transformation is done by the Kubelka-Munk conversion.[49] The value of the optical band gap can be found from the interception of the two tangent lines of the absorption spectrum.

4. Differential scanning calorimetry

The phase transition of α-Ag_3VO_4 was studied by differential scanning calorimetry (Mettler-Toledo DSC 822e). (See Fig. 7.) Indium and zinc references were used to calibrate the heat changes. A small amount of sample (3–4 mg) was sealed in an aluminum pan and heated at 10 °C/min to 400 °C under dry flowing N_2 gas (55 mL/min). The heating and cooling graphs are both recorded. There is a 25-K hysteresis difference between the phase transition between heating and cooling.

[*]Present address: Oak Ridge National Laboratory, Oak Ridge, TN 37831 (USA).

[1]*Handbook of Transparent Conductors*, edited by David S. Ginley, Hideo Hosono, and David C. Paine (Springer, New York, 2011).

[2]S. Lany and A. Zunger, Phys. Rev. Lett. **98**, 045501 (2007).

[3]A. Zunger, Appl. Phys. Lett. **83**, 57 (2003).

[4]R. E. Steuer, *Multiple Criteria Optimization: Theory, Computations, and Application* (Wiley, New York, 1986).

[5]H. Kawazoe, M. Yasukawa, H. Hyodo, M. Kurita, H. Yanagi, and H. Hosono, Nature (London) **389**, 939 (1997).

[6]R. Nagarajan, A. D. Draeseke, A. W. Sleight, and J. Tate, J. Appl. Phys. **89**, 8022 (2001).

[7]K. Ueda, T. Hase, H. Yanagi, H. Kawazoe, H. Hosono, H. Ohta, M. Orita, and M. Hirano, J. Appl. Phys. **89**, 1790 (2001).

[8]H. Yanagi, T. Hase, S. Ibuki, K. Ueda, and H. Hosono, Appl. Phys. Lett. **78**, 1583 (2001).

[9]N. Duan, A. W. Sleight, M. K. Jayaraj, and J. Tate, Appl. Phys. Lett. **77**, 1325 (2000).

[10]A. Kudo, H. Yanagi, H. Hosono, and H. Kawazoe, Appl. Phys. Lett. **73**, 220 (1998).

[11]K. Ueda, H. Hiramatsu, H. Ohta, M. Hirano, T. Kamiya, and H. Hosono, Phys. Rev. B **69**, 155305 (2004).

[12]H. Hiramatsu, H. Yanagi, T. Kamiya, K. Ueda, M. Hirano, and H. Hosono, Chem. Mater. **20**, 326 (2008).

[13]M.-L. Liu, L.-B. Wu, F.-Q. Huang, L.-D. Chen, and I.-W. Chen, J. Appl. Phys. **102**, 116108 (2007).

[14]D. O. Scanlon and G. W. Watson, Chem. Mater. **21**, 5435 (2009).

[15]G. Bergerhoff and I. D. Brown, in *Crystallographic Databases*, edited by F. H. Allen *et al*. (Hrsg.) Chester, International Union of Crystallography (1987).

[16]A. Belsky, M. Hellenbrandt, Karen V. L., and P. Luksch, Acta Crystallogr. Sect. B **58**, 364 (2002).

[17]J. Osorio-Guillen, S. Lany, S. V. Barabash, and A. Zunger, Phys. Rev. Lett. **96**, 107203 (2006).

[18]C. Persson, Y.-J. Zhao, S. Lany, and A. Zunger, Phys. Rev. B **72**, 035211 (2005).

[19]S. Lany and A. Zunger, Phys. Rev. B **78**, 235104 (2008).

[20]H. Raebiger, S. Lany, and A. Zunger, Phys. Rev. B **76**, 045209 (2007).

[21]M. Shishkin and G. Kresse, Phys. Rev. B **74**, 035101 (2006).

[22]S. B. Rivers, G. Bernhardt, M. W. Wright, D. J. Frankel, M. M. Steeves, and R. J. Lad, Thin Solid Films **515**, 8684 (2007).

[23]J. D. Perkins, T. R. Paudel, A. Zakutayev, P. Ndione, P. A. Parilla, D. L. Young, S. Lany, D. S. Ginley, A. Zunger, N. H. Perry, Y. Tang, M. Grayson, T. O. Mason, J. S. Bettinger, Y. Shi, and M. F. Toney, (unpublished).

[24]R. E. Dinnebier, A. Kowalevskyy, H. Reichert, and M. Jansen, Z. Kristallogr. **222**, 420 (2007).

[25]T. A. Albrecht, C. L. Stern, and K. R. Poeppelmeier, Inorg. Chem. **46**, 1704 (2007).

[26]E. Parthe', *Crystal Chemistry of Tetrahedral Structures* (Gordon and Breach, New York, 1964).

[27]A. A. Mbaye, D. M. Wood, and Alex Zunger, Phys. Rev. B **37**, 3008 (1988).

[28]T. Hirono, H. Koizumi, T. Yamada, and T. Nishi, Thin Solid Films **149**, L85 (1987).

[29]N. Barrier, M. Hervieu, N. Nguyen, and B. Raveau, Solid State Sci. **10**, 137 (2008).

[30]A. Rabenau, Angew. Chem., Int. Ed. Engl. **24**, 1026 (1985).

[31]T. Hirono and T. Yamada, J. Appl. Phys. **55**, 781 (1984).

[32]M. V. Fischetti and S. E. Laux, J. Appl. Phys. **80**, 2234 (1996).

[33]G. Ottaviani, L. Reggiani, C. Canali, F. Nava, and A. Alberigi-Quaranta, Phys. Rev. B **12**, 3318 (1975).

[34]N. W. Ashcroft and N. D. Mermin, *Solid State Physics* (Saunders College Publishing, 1976).

[35]G. Grosso and G. Pastori Parravicini, *Solid State Physics* (Academic, New York, 2000).

[36]S. L. Dudarev, G. A. Botton, S. Y. Savrasov, C. J. Humphreys, and A. P. Sutton, Phys. Rev. B **57**, 1505 (1998).

[37]G. Kresse and J. Hafner, Phys. Rev. B **47**, 558 (1993).

[38]G. Kresse and J. Furthmuller, Phys. Rev. B **54**, 11169 (1996).

[39]S. Lany, J. Osorio-Guillen, and A. Zunger, Phys. Rev. B **75**, 241203(R) (2007).

[40]S. Lany, Phys. Rev. B **78**, 245207 (2008).

[41]Giovanni Onida, Lucia Reining, and Angel Rubio, Rev. Mod. Phys. **74**, 601 (2002).

[42]M. van Schilfgaarde, Takao Kotani, and S. Faleev, Phys. Rev. Lett. **96**, 226402 (2006).

[43]F. Fuchs, J. Furthmüller, F. Bechstedt, M. Shishkin, and G. Kresse, Phys. Rev. B **76**, 115109 (2007).

[44]M. Shishkin, M. Marsman, and G. Kresse, Phys. Rev. Lett. **99**, 246403 (2007).

[45]J. Paier, M. Marsman, and G. Kresse, Phys. Rev. B **78**, 121201 (2008).

[46]F. Bechstedt, F. Fuchs, and G. Kresse, Phys. Status Solidi **246**, 1877 (2009).

[47]S. Lany, H. Raebiger, and A. Zunger, Phys. Rev. B **77**, 241201 (2008).

[48]A. F. Wells, *Structural Inorganic Chemistry* (Clarendon, Oxford, UK, 1975).

[49]P. Kubelka and F. Munk, Z. Tech. Phys. **12**, 593 (1931).